IOPscience iopscience.iop.org

Home Search Collections Journals About Contact us My IOPscience

The construction of a quantum Markov partition

This article has been downloaded from IOPscience. Please scroll down to see the full text article.

1999 J. Phys. A: Math. Gen. 32 7273

(http://iopscience.iop.org/0305-4470/32/42/304)

View the table of contents for this issue, or go to the journal homepage for more

Download details:
IP Address: 171.66.16.111
The article was downloaded on 02/06/2010 at 07:47

Please note that terms and conditions apply.

J. Phys. A: Math. Gen. **32** (1999) 7273–7286. Printed in the UK PII: S0305-4470(99)04094-9

The construction of a quantum Markov partition

Raúl O Vallejos† and Marcos Saraceno‡

† Instituto de Física, Universidade do Estado do Rio de Janeiro, Rua São Francisco Xavier 524, CEP 20559-900 Rio de Janeiro, Brazil
‡ Departamento de Física, Comisión Nacional de Energía Atómica, Avenida del Libertador 8250, 1429 Buenos Aires, Argentina

E-mail: raul@dfnae1.fis.uerj.br and saraceno@tandar.cnea.gov.ar

Received 7 May 1999, in final form 9 September 1999

Abstract. We present a method for constructing a quantum Markov partition. Its elements are obtained by quantizing the characteristic function of the classical rectangles. The result is a set of quantum operators which behave asymptotically as projectors over the classical rectangles apart from edge and corner effects. We investigate their spectral properties and different methods of construction. The quantum partition is shown to induce a symbolic decomposition of the quantum evolution operator. In particular, an exact expression for the traces of the propagator is obtained having the same structure as the Gutzwiller periodic orbit sum.

1. Introduction

For classical hyperbolic systems, symbolic dynamics provides the proper coordinates for an efficient description of chaotic behaviour [1,2]. Such a description does not exist at the quantum level (with the exception of a few important semiclassical treatments [3]). This work is an attempt to apply the techniques of symbolic dynamics in quantum mechanics. The ultimate goal of this kind of investigation is to rewrite the equations of quantum mechanics in terms of adequate symbols for a given (chaotic) problem.

The basic idea of symbolic dynamics is to encode a dynamical trajectory as an infinite sequence of symbols in order that there is a correspondence between properties of the actual motion, e.g., periodicity, and properties of the symbolic motion. The association between phase space coordinates and symbols is made with the help of a partition of phase space (details are presented in section 4). We are thus faced with the problem of defining properly the quantum analogues to bounded regions of phase space. The essential difficulties in doing this are the limitations imposed by the uncertainty principle. Strictly speaking, quantum mechanics is not only in contradiction with the notion of a phase space point but also with that of a finite subset of phase space.

In a previous paper [4] a symbolic decomposition along these lines was studied, but no special constructions were necessary because the invariant manifolds were aligned with the coordinate axes, thus turning the elements of the partition into simple projectors. Here we generalize the method of [4] by constructing certain objects (we call them *quantum rectangles*) which are the quantum equivalents to the classical elements of a Markov partition. Then we investigate their properties and different possibilities for their construction. The quantum rectangles behave approximately as projectors over the corresponding classical regions apart from diffraction effects which are characteristic of quantum phenomena.

0305-4470/99/427273+14$30.00 © 1999 IOP Publishing Ltd

Once the quantum rectangles have been defined, it is straightforward to construct a quantum Markov partition. In perfect analogy with the classical case, this partition leads to a symbolic decomposition of the propagator. Eventually, we obtain an *exact* trace formula having the same structure as Gutzwiller's.

The rest of the paper is structured as follows. In section 2 we argue that the quantum analogue of a finite region of phase space can be constructed in a natural way by simply quantizing the characteristic function of that region. In section 3 we show that in the semiclassical limit the quantized regions display properties consistent with the classical ones. Section 4 describes the application of the quantum Markov partition to decompose the propagator. Finally, section 5 contains the concluding remarks.

2. Construction

The first step towards the construction of a quantum Markov partition consists of defining the quantum analogue for a finite region R of the classical phase space (to be considered later as belonging to the partition). For the sake of simplicity, we restrict our analysis to two-dimensional phase spaces with the topology of a torus (we further assume that this is the usual unit torus $T^2 = S^1 \times S^1$). Extensions to spaces of higher dimensionality or to other topologies can also be considered. We want to construct an operator which is the quantization of the characteristic function χ_R of the region R,

$$\chi_R(q, p) = \begin{cases} 1 & \text{if } (q, p) \in R \\ 0 & \text{otherwise.} \end{cases} \tag{1}$$

Let us just mention two simple properties of the characteristic functions: distributivity with respect to the set intersection and normalization

$$\chi_{R_1}\chi_{R_2} = \chi_{R_1 \cap R_2} \tag{2}$$

$$\int \mathrm{d}p\, \mathrm{d}q\, \chi_R(p, q) = \mathcal{A}_R \tag{3}$$

the integral is over the torus and $\mathcal{A}_R$ is the area (volume) of the region R. For the moment these regions are arbitrary but eventually they will become the elements of a partition of the phase space.

To establish the connection with quantum mechanics we make use of a phase space representation, that is, a basis $\{\hat{B}(q_k, p_j), 1 \leqslant k, j \leqslant N\}$ for operators acting on the Hilbert space $\mathcal{H}$ of dimension $N = 1/(2\pi\hbar)$. The q and p representations on the torus are discrete, and mutually related through a discrete Fourier transform [7]:

$$\langle p_j | q_k \rangle = \frac{1}{\sqrt{N}} \exp(-2\pi \mathrm{i} N p_j q_k). \tag{4}$$

Any operator $\hat{O}$ can be written as a linear combination of the elements of the basis

$$\hat{O} = \sum_{k,j=1}^{N} O(q_k, p_j)\hat{B}(q_k, p_j). \tag{5}$$

Conversely, for a given symbol $O(q_k, p_j)$, equation (5) defines an operator $\hat{O}$. We require the operator basis to decompose the identity

$$\sum_{k,j=1}^{N} \hat{B}(q_k, p_j) \propto \mathbb{1}_{\mathcal{H}}. \tag{6}$$

Two examples of operator bases will be considered: The Kirkwood representation, associated to the basis $\{|q_k\rangle\langle q_k|p_j\rangle\langle p_j|\}$, and a representation of projectors over coherent states, $\{|q_k + \mathrm{i}p_j\rangle\langle q_k + \mathrm{i}p_j|\}$. In both cases the discretization used is $q_k = k/N$ and $p_j = j/N$, $1 \leqslant k, j \leqslant N$, corresponding to periodic boundary conditions on the torus. To construct the set of coherent states we start from a circular Gaussian packet centred at $(\frac{1}{2}, \frac{1}{2})$, say in the q representation. Then, this function is evaluated in the discrete q mesh and normalized. The whole set of coherent states is obtained by successive translations of the initial state to all the points (q_k, p_j) of the mesh [5].

Both representations allow a natural construction of the quantization $\hat{R}$ of a phase space region R:

$$\hat{R}_K = \sum_{k,j=1}^{N} \chi_R(q_k, p_j)|q_k\rangle\langle q_k|p_j\rangle\langle p_j| \tag{7}$$

$$\hat{R}_z = \frac{1}{N}\sum_{k,j=1}^{N} \chi_R(q_k, p_j)|q_k + \mathrm{i}p_j\rangle\langle q_k + \mathrm{i}p_j|. \tag{8}$$

The normalizations are such that the operator associated to the whole torus is the identity $\mathbb{1}_{\mathcal{H}}$ in both cases. The factor $1/N$ in the coherent case is due to the overcompleteness of that representation. While $\hat{R}_z$ is Hermitian and treats symmetrically p and q, $\hat{R}_K$ is not. Therefore, in applications we use the symmetrical combination

$$\hat{R}^s_K = (\hat{R}_K + \hat{R}^\dagger_K)/2 \tag{9}$$

(we come back to this point later).

Because of the phase space construction, we expect that the quantization of the characteristic functions that we have adopted will yield operators that are approximately projectors on the classical regions and that this correspondence will improve as $N \to \infty$. However, the construction is representation dependent, and treats differently the quantum diffraction effects produced by the edges and corners of the classical region. We will show that the Gaussian region $\hat{R}_z$ tends smoothly to its classical counterpart. On the other hand, the convergence of $\hat{R}_K$, which has been constructed from a sharp distribution, shows characteristic rapid oscillatory structure.

3. Properties

The spectral analysis of the quantum rectangles are the key to understanding their general properties. Given that analytical studies seem extremely difficult, we resorted to numerical calculations: after choosing a classical region R, we used the defining equations (7)–(9) to construct the matrices of the operators $\hat{R}_z$ and $\hat{R}^s_K$, say in the q representation. As an example, let us exhibit the case of a quantum rectangle defined through the Kirkwood representation:

$$\langle q_k|\hat{R}_K|q_l\rangle = \sum_{j=1}^{N} \chi_R(q_k, p_j)\langle q_k|p_j\rangle\langle p_j|q_l\rangle. \tag{10}$$

The equation above shows that the matrix of $\hat{R}_K$ is just the product of two simple matrices: the usual Fourier matrix (4), and a Fourier matrix $\langle q_k|p_j\rangle$ in which those elements 'outside the region R' have been substituted by zeros (this operation is done by the characteristic function χ_R). The matrix of the Gaussian rectangle $\hat{R}_z$ does not admit such a simple expression, but it can also be easily constructed—one only needs the elements $\langle q_l|q_k + \mathrm{i}p_j\rangle$ (see [5]). In both cases, eigenvalues and eigenvectors are obtained by numerical diagonalization of a complex Hermitian matrix of dimension $N = 1/h$ (in our examples $90 \leqslant N \leqslant 240$).

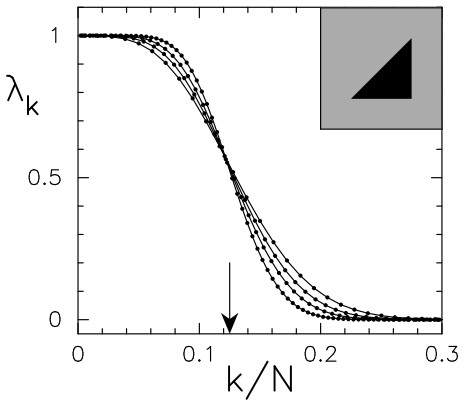

Figure 1. Eigenvalues of a triangular region (inset) constructed from the coherent basis. We plot the eigenvalues λ_k as a function of the normalized eigenvalue number k/N, where $N = 1/(2\pi\hbar)$ is the semiclassical parameter. We have considered $N = 90, 120, 160, 240$. As N grows the distribution of eigenvalues tends to a step function, the position of the step being determined by the area of the classical region which is $\frac{1}{8} = 0.125$ (indicated with an arrow). Curves have been drawn to guide the eye.

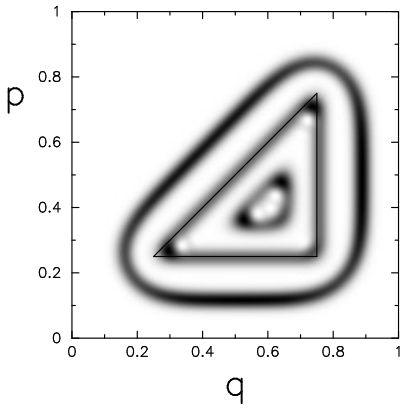

Figure 2. Husimi representation of three eigenfunctions of the triangular region of figure 1. (This is a linear grey plot, with black and white corresponding to the highest and smallest amplitudes, respectively.) The associated eigenvalues are $\lambda_k = 1.000, 0.498, 0.728 \times 10^{-12}$; respectively $k = 4, 31, 90$ ($N = 240$). The border of the classical region is shown for reference (full black line).

We begin by discussing our numerical results for the Gaussian regions. For the case in which R is a triangle, figure 1 shows the way in which $\hat{R}_z$ behaves in the limit $N \to \infty$. There we plot the eigenvalues λ_k (associated to the eigenvectors $|\psi_k\rangle$) in decreasing order. Most of the eigenvalues take the values ≈ 0 or ≈ 1. Intermediate values exist, but their *relative* number goes to zero in the semiclassical limit. Therefore, semiclassically $\hat{R}_z$ behaves as a projector on the triangle. Figure 2 shows that the Husimi representations $|\langle q + \mathrm{i}p|\psi\rangle|^2$ of the corresponding eigenfuctions are localized on nested triangles concentrically with the boundary of the classical region. The situation is very similar to that of integrable Hamiltonians, where the Husimi density of an eigenfunction is localized over the associated quantized torus and decays exponentially as one moves away from the torus. Exploiting this analogy we can derive a semiclassical quantization rule for the eigenvalues and eigenfunctions of a quantum region. Notice first that the eigenvalue equation for $\hat{R}_z$ is

$$\frac{1}{N}\sum_{(q,p)} \chi_R |q + \mathrm{i}p\rangle\langle q + \mathrm{i}p|\psi_k\rangle = \lambda_k |\psi_k\rangle \tag{11}$$

implying that

$$\frac{1}{N}\sum_{(q,p)\in R} |\langle q + \mathrm{i}p|\psi_k\rangle|^2 = \lambda_k \tag{12}$$

(if the sum were unrestricted the LHS above would be equal to one). Let us now make the following assumptions. Sums can be substituted by integrals (we are interested in the limit $N \to \infty$). The Husimi of the kth eigenfunction is associated to a quantized 'torus' lying at a distance d_k from the border of the region. Finally, in the direction perpendicular to the torus, $\hat{y}$ ($y = 0$ on the border of the the region), the Husimi is a normalized Gaussian:

$$|\langle q + \mathrm{i}p|\psi_k\rangle|^2 \propto \exp[-(y - d_k)^2/\hbar]/\sqrt{\pi\hbar} \tag{13}$$

($d_k < 0$ if the torus lies inside the region). Combining equations (12), (13) we arrive at the semiclassical quantization rule

$$\lambda_k \approx \int_{-\infty}^{0} \mathrm{d}y \, \frac{1}{\sqrt{\pi\overline{h}}} \exp[-(y-d_k)^2/\overline{h}] = \frac{1}{2} - \frac{1}{2}\,\mathrm{erf}\left(\frac{d_k}{\sqrt{\overline{h}}}\right). \tag{14}$$

To determine d_k we approximate each quantized torus by a scaled image of the border of the region, and set the area between two consecutive tori to $2\pi\overline{h}$. We give expressions for d_k for the simplest shaped regions: a square, the triangle of figure 1, and a circle

$$d_k = \begin{cases} \dfrac{\sqrt{k\overline{h}} - L}{2} & \text{square} \\ \dfrac{\sqrt{2k\overline{h}} - L}{2+\sqrt{2}} & \text{triangle} \\ \sqrt{\dfrac{k\overline{h}}{\pi}} - R & \text{circle} \end{cases} \tag{15}$$

where R is the radius of the circle and L is the side of both the square and the triangle (see the inset of figure 3).

In figure 3 we compare the analytical expression (14) with the numerical results for $N = 90$ and three different regions, verifying that the agreement is very good. However, some deviations can still be observed which we associate with the relatively small value of N. These deviations are more important in the case of the triangle (e.g., around $k = 22$) because of its smaller area and acute corners. In particular, our numerical results, well described by (14), show that the width of the transition region from 1 to 0 is independent of $\overline{h}$; in other words, the relative number of border eigenstates goes to zero as $1/N$. In this sense we say that the quantum regions behave as projectors in the semiclassical limit.

The quantization of classical regions with sharp boundaries by way of the coherent states presented above has the advantage of producing very smooth and analytically understandable results. The sharp edges are blurred by the Gaussian smoothing and the resulting quantum rectangles are always 'soft' on the scale of $\overline{h}$.

Other representations, namely Kirkwood and Wigner [6], allow higher definition but display characteristic diffraction effects at the edges and corners. Figure 4 shows the eigenvalues of the operator $\hat{R}_K^s$ of the triangular region. Notice that the distribution of eigenvalues is not smooth as in the coherent case but presents a singularity associated to boundary effects. This singularity is inherent to the sharpness of the Kirkwood construction and is also displayed by the non-Hermitian rectangles $\hat{R}_K$ and $\hat{R}_K^\dagger$ (not shown). Some typical eigenfunctions are also displayed (inset). In this case, the eigenfunctions do not present the high degree of symmetry of the coherent case, but are rather irregular. The eigenvalue still determines the localization of the eigenfunction with respect to the border ($<\frac{1}{2}$, interior; $>\frac{1}{2}$, exterior). However, as the eigenfunctions are not nested like in the coherent case, the ordering is not always unambiguous. Except for this irregularity, the Kirkwood rectangles behave asymptotically in the same way as the coherent ones: i.e., they tend to projectors over the classical regions. The analytical treatment of the diffraction effects (see [17]) is more involved and we do not attempt it at this time.

Besides the nice spectral behaviour discussed above, the quantum rectangles (either coherent or Kirkwood) should display some additional properties for our construction to be consistent.

(i) How does one define the 'area' of a quantum region? In order to quantify the dissipation of a quantum Smale-horseshoe map, we argued in [8] that the usual operator norm $\mathrm{Tr}(\hat{R}\hat{R}^\dagger)/N$ is a reasonable definition of area. For the Kirkwood rectangles $\hat{R}_K$ it is easy to prove that

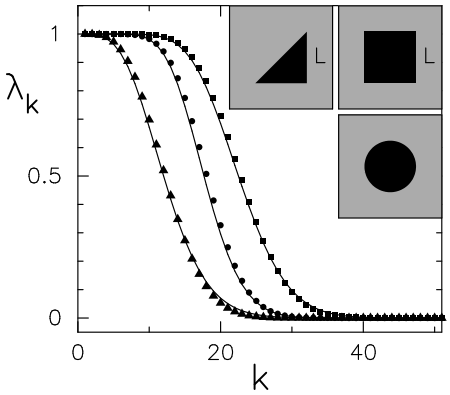

Figure 3. Eigenvalues of three regions: triangle, square, and circle (inset). There is a one-to-one correspondence between graphical symbols and regions. The full curves are the analytical distributions discussed in the text ($N = 90$).

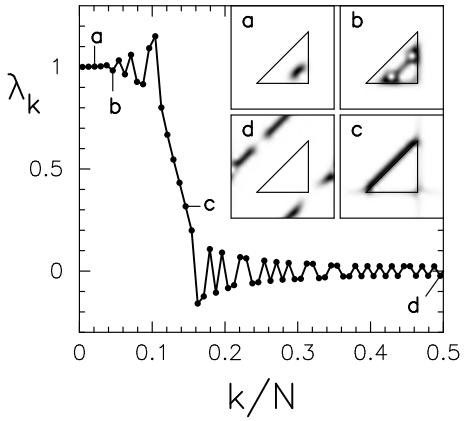

Figure 4. Eigenvalues of a triangular region quantized from the Kirkwood basis, and four eigenfunctions (Husimi representation, linear grey plot). The ordering of the eigenvalues is such that the parameter $|1 - |\lambda_k||$ increases to the right. The eigenfunctions labelled a–d correspond to the eigenvalues $\lambda_k = 1.002, 0.983, 0.317, -0.023$ ($k = 3, 6, 18, 60$), respectively ($N = 120$).

this definition coincides exactly with the classical area $\mathcal{A}_R$. Alternatively one could simply define the area as $\mathrm{Tr}\,\hat{R}/N$, in which case classical and quantum areas are identical for both representations. Anyway, as $\hat{R}$ tends to a projector

$$\mathrm{Tr}(\hat{R}\hat{R}^\dagger)/N \approx \mathrm{Tr}\,\hat{R}/N = \mathcal{A}_R. \tag{16}$$

Thus both expressions are acceptable definitions of quantum area.

(ii) For the study of spectral properties the Hermitian operator $\hat{R}_K^s$ was preferred to the non-Hermitian $\hat{R}_K$ and $\hat{R}_K^\dagger$. The latter are more appropriate for the decomposition of the propagators we present in section 4. However, in the limit $\mathcal{A}_R \gg \overline{h}$, $\hat{R}_K$ and $\hat{R}_K^\dagger$ will be approximately equal, given that they only differ in the ordering of q and p. Then $\hat{R}_K$, $\hat{R}_K^\dagger$, and $\hat{R}_K^s$ are semiclassically equivalent.

(iii) Quantization and propagation must commute. If U is a classical simplectic map and $\hat{U}$ its quantization, then

$$\hat{U}^T \hat{R} \hat{U}^{-T} \to \widehat{U^T(R)} \tag{17}$$

where it is understood that one must fix T and take the limit $\overline{h} \to 0$. We illustrate this point in figure 5, where the rectangle R_1 of the Markov partition for the cat map [11] is propagated once by the quantum cat map [13]. Notice that the bulk classical behaviour is correctly reproduced and that additional diffraction effects are visible in figure 5(a), while the coherent rectangle in figure 5(b) is much smoother.

(iv) We also expect quantization to commute with the classical set operations:

$$\widehat{R_1 \cap R_2} \approx \hat{R}_1 \hat{R}_2 \approx \hat{R}_2 \hat{R}_1 \tag{18}$$

$$\widehat{R_1 \cup R_2} \approx \hat{R}_1 + \hat{R}_2 - \hat{R}_1 \hat{R}_2. \tag{19}$$

An instance of equation (18) which is of special interest for the construction of a partition is that of two adjacent regions, i.e. two regions whose intersection is a line segment. Consider

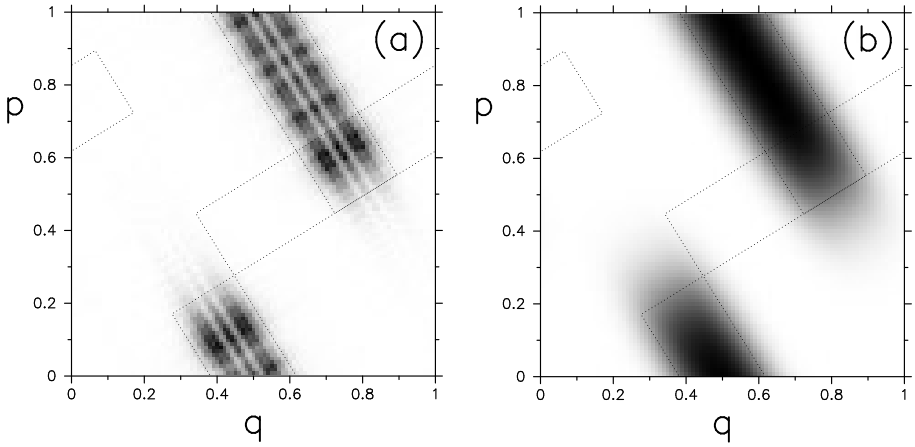

Figure 5. (*a*) Propagation of a Kirkwood rectangle. We show a linear grey plot of $|\langle p|\hat{U}^{\dagger}\hat{R}_{1K}\hat{U}|q\rangle|$, where R_1 is one of the five elements of the Markov partition of Arnold's cat map (see figure 6) and $\hat{U}$ is the quantized cat map (section 4). Compare this with the boundaries of the classically propagated rectangle, $U^{-1}(R_1)$ (dots). For the sake of future referencing we also display the boundary of the element R_5 (dots). (*b*) As before but for the coherent rectangle $\hat{R}_{1z}$. Now we plot the operator symbol $\langle q+\mathrm{i}p|\hat{U}^{\dagger}\hat{R}_{1z}\hat{U}|q+\mathrm{i}p\rangle$. In both cases the dimension of the Hilbert space is $N = 100$.

the spectral decomposition of two such regions $\hat{R}_1$ and $\hat{R}_2$:

$$\hat{R}_i = \sum_{k=1}^{N} \lambda_{ik}|\psi_{ik}\rangle\langle\psi_{ik}| \qquad i = 1, 2. \tag{20}$$

To quantify the overlap of these regions we calculate the quantum area of the product (intersection) operator:

$$\frac{1}{N}\,\mathrm{Tr}\,\hat{R}_1\hat{R}_2 = \frac{1}{N}\sum_{k,k'=1}^{N} \lambda_{1k}\lambda_{2k'}^{*}|\langle\psi_{1k}|\psi_{2k'}\rangle|^2. \tag{21}$$

Now recall the picture of eigenstates localized on scaled images of the border of a region. If $|\psi_{1k}\rangle$ and $|\psi_{2k'}\rangle$ are not both localized on the respective borders of R_1 and R_2, the product $\lambda_{1k}\lambda_{2k'}$ will be exponentially small. But we have seen that the number of border eigenstates is of the order of one, implying that the quantum area is of order $1/N$. Thus the intersection of adjacent quantum regions is semiclassically negligible. (If the regions are a finite distance apart, the quantum intersection tends exponentially to zero when $N \to \infty$.) Even though we lack an analytical description of the spectral properties of the Kirkwood case, our numerical experience shows that, due to the very similar localization properties, Kirkwood rectangles behave qualitatively in the same way.

In the next section we show an application of the quantum regions which provides additional support to the statements above.

4. Symbolic decomposition of the traces of the propagator

Before discussing the applications of the quantum rectangles in quantum dynamics, we present a short reminder of classical symbolic dynamics in a setting appropriate to the transition to quantum mechanics. We only consider here the symbolic dynamics associated with a finite Markov partition. A Markov partition for a hyperbolic map U consists of a set of regions

$R_1, R_2, \ldots, R_P$ (usually called 'rectangles') which satisfy the following properties. The boundaries of R_i are defined by segments of the expanding and contracting manifolds of U. Whenever $U(R_i)$ intersects the interior of R_j, the image cuts completely across R_j in the unstable direction. Similarly, the backwards image $U^{-1}(R_i)$ cuts completely across the other rectangles along the stable direction [1, 2].

From the Markov partition, successively finer partitions can be obtained by intersecting the elements of the basic partition with its positive and negative images by the map (product partition):

$$R_{\epsilon_{-K}\ldots\epsilon_{-1}\cdot\epsilon_0\epsilon_1\ldots\epsilon_M} = \bigcap_{s=-K}^{s=M} U^s(R_{\epsilon_s}) \tag{22}$$

where ϵ_s can take any of the values $1, 2, \ldots P$. Each element of the new partition can be labelled by a different symbolic code

$$\nu(-K, M) = \epsilon_{-K}\ldots\epsilon_{-1}\cdot\epsilon_0\epsilon_1\ldots\epsilon_M. \tag{23}$$

As the original rectangles, the refined rectangles above possess the property of decomposing the phase space into disjoint regions (we do not take into account borders, which are zero-measure). When acting on these rectangles, the map is simply a *shift*:

$$U^{-1}(R_{\epsilon_{-K}\ldots\epsilon_{-1}\cdot\epsilon_0\epsilon_1\ldots\epsilon_M}) = R_{\epsilon_{-K}\ldots\epsilon_0\cdot\epsilon_1\ldots\epsilon_M}. \tag{24}$$

From the properties of the Markov partitions, it can be proven that in the limit $K, M \to \infty$ the intersections of (22) are either a single point or the empty set [2]. The latter possibility means that the transitions between certain pairs of basic regions are prohibited; the information about allowed and prohibited sequences can be enclosed in a transition matrix

$$t_{ij} = \begin{cases} 1 & \text{if} \quad U(R_i)\cap R_j \neq \emptyset \\ 0 & \text{otherwise.} \end{cases} \tag{25}$$

In this way, the Markov partition allows for setting up a one-to-one correspondence between phase space points and *allowed* sequences of symbols.

The existence of a symbolic dynamics allows for an exhaustive coding of the orbits of the map. In particular, periodic orbits are in correspondence with the periodic sequences of the same periodicity. Given an arbitrary system, it is a hard task to decide if it admits a symbolic dynamics; even if it does, the translation from symbols to phase space coordinates is in general extremely difficult. The example we will consider (the cat map) does not present any of these difficulties, thus eliminating non-essential complications.

In the following we show how the symbolic dynamics of a classical map can be used to decompose the traces of the quantized map. The quantum analogues of the elements of the classical Markov partition are the quantum rectangles $\hat{R}$ described in sections 2 and 3. The quantum partitions are obtained by translating to quantum mechanics the steps in the construction of the classical ones. Starting from the quantizations of the regions of the classical basic partition, we define the quantum refinement in two steps. First, the regions (quantum 'projectors') are propagated using the Heisenberg equations of motion. Then, noting that 'intersections' of quantum rectangles correspond to matrix multiplications, we arrive at a quantum product partition with elements written as a time-ordered multiplication of matrices

$$\begin{aligned}\hat{R}_{\nu(-K,M)} &= \hat{U}^{-K}\hat{R}_{\epsilon_{-K}}\hat{U}^{K}\ldots\hat{U}^{M}\hat{R}_{\epsilon_M}\hat{U}^{-M} \\ &= \hat{U}^{-K}\hat{R}_{\epsilon_{-K}}\hat{U}\hat{R}_{\epsilon_{-K+1}}\ldots\hat{R}_{\epsilon_{M-1}}\hat{U}\hat{R}_{\epsilon_M}\hat{U}^{-M}.\end{aligned} \tag{26}$$

The counterpart of the classical decomposition of the phase space is the quantum decomposition of the identity

$$\sum_{\nu(-K,M)} \hat{R}_{\nu(-K,M)} = \mathbb{1}_{\mathcal{H}}. \tag{27}$$

The quantum propagation is also a *shift*:

$$\hat{U}^{-1}\hat{R}_{\epsilon_{-K}\ldots\epsilon_{-1}\cdot\epsilon_0\epsilon_1\ldots\epsilon_M}\hat{U} = \hat{R}_{\epsilon_{-K}\ldots\epsilon_0\cdot\epsilon_1\ldots\epsilon_M}. \tag{28}$$

Even though the quantum rectangles do not have zero 'intersection', the product of two elements of the partition is semiclassically negligible. Finally, when $N \to \infty$ with K and M fixed, the quantum rectangles tend to the classical ones. The precise meaning of these limits, and the way they are achieved, were discussed in section 3.

The key property of the quantum partition we have constructed is the symbolic decomposition of the traces of the propagator. Consider the discrete path sum for the trace of a power of the propagator in the coherent state representation

$$\mathrm{Tr}\,\hat{U}^L = \frac{1}{N^L}\sum\langle\alpha_0|\hat{U}|\alpha_{L-1}\rangle\langle\alpha_{L-1}|\hat{U}\ldots|\alpha_1\rangle\langle\alpha_1|\hat{U}|\alpha_0\rangle \tag{29}$$

where the sum runs over all the *closed* paths $\alpha_0, \alpha_1, \ldots, \alpha_{L-1}, \alpha_L \equiv \alpha_0$, which are discrete both in time and in the coordinates (we recall that $\alpha \equiv q + \mathrm{i}p$ moves on the discrete q–p grid). Semiclassically, the trace of $\hat{U}^L$ will be dominated by the periodic trajectories (of period L) of the classical map U and their neighbouring paths. The Markov partition allows us to stick symbolic labels not only to trajectories but also to paths. So, one has a natural way of dividing the space of paths into disjoints subsets, each one characterized by a symbol ν of length L and containing the periodic trajectory associated with ν. This observation allows us to reorganize the sum in (29) in the following way. Sum first over paths having the same symbolic code $\nu = \epsilon_0\epsilon_1\ldots\epsilon_{L-1}$, i.e. such that $\alpha_0 \in R_{\epsilon_0}$, $\alpha_1 \in R_{\epsilon_1}$, etc. Then sum over all ν:

$$\mathrm{Tr}\,\hat{U}^L = \frac{1}{N^L}\,\mathrm{Tr}\sum_{\nu}\sum_{\alpha_0\in R_{\epsilon_0}}\cdots\sum_{\alpha_{L-1}\in R_{\epsilon_{L-1}}}\hat{U}|\alpha_{L-1}\rangle\langle\alpha_{L-1}|\hat{U}\ldots\hat{U}|\alpha_0\rangle\langle\alpha_0|. \tag{30}$$

But the inner sums define the quantum rectangles, then

$$\mathrm{Tr}\,\hat{U}^L = \mathrm{Tr}\sum_{\nu}\hat{U}\hat{R}_{\epsilon_{L-1}}\ldots\hat{U}\hat{R}_{\epsilon_1}\hat{U}\hat{R}_{\epsilon_0} \equiv \sum_{\nu}\mathrm{Tr}\,\hat{U}_{\nu}^L. \tag{31}$$

Thus the mechanism of path grouping is automatically implemented by the quantum 'projectors' over the classical rectangles. Equation (31) is completely equivalent to (29), the only difference being the grouping of closed paths into families sharing the same symbolic code ν. Each one of these families contributes to a partial trace $\mathrm{Tr}\,\hat{U}_{\nu}^L$. Analogous results are obtained in the Kirkwood case. In fact, starting from a path sum in the Kirkwood representation,

$$\mathrm{Tr}\,\hat{U}^L = \sum\langle q_0|p_0\rangle\langle p_0|\hat{U}\ldots\hat{U}|q_2\rangle\langle q_2|p_2\rangle\langle p_2|\hat{U}|q_1\rangle\langle q_1|p_1\rangle\langle p_1|\hat{U}|q_0\rangle \tag{32}$$

one arrives at the same result of equation (31) but with the Kirkwood rectangles instead of the coherent ones. Using the cyclic property, the partial traces of (31) (or the Kirkwood counterparts) can be rewritten in terms of the refined rectangles of equation (26)

$$\mathrm{Tr}\,\hat{U}^L_{\nu(-K,M)} = \mathrm{Tr}[\hat{U}^L\hat{R}_{\nu(-K,M)}]. \tag{33}$$

The integers K, M must satisfy $K + M = L - 1$, but are otherwise arbitrary. By varying K and M (L fixed) one constructs different types of rectangles, e.g., the choice $K = 0$, $M = L - 1$ produces 'unstable' rectangles (stretched along the unstable manifolds)

$$\hat{R}_{\cdot\epsilon_0\epsilon_1\ldots\epsilon_{L-1}} = \hat{R}_{\epsilon_0}\hat{U}^1\hat{R}_{\epsilon_1}\hat{U}^{-1}\ldots\hat{U}^{L-1}\hat{R}_{\epsilon_L}\hat{U}^{-(L-1)}. \tag{34}$$

Similarly, with $M = 0$ and $K = L - 1$, 'stable' rectangles are obtained. Anyway, stable and unstable rectangles are related by the unitary transformation (28), ensuring that $\mathrm{Tr}\,\hat{U}^L_{\nu(-K,M)}$ does not depend on the particular choice of K, M. Moreover, it is satisfactory to verify that the trace of $\hat{U}^L_{\nu}$ remains unchanged under cyclical shifts of the 'bits' $\epsilon_0\epsilon_1\ldots\epsilon_{L-1}$ of ν (as is

obvious from (31)); this is a reflection of the classical invariance property: by shifting the bits of ν one just moves around the periodic trajectory ν.

The refined rectangle $\hat{R}_{\nu(-K,M)}$ has as its classical limit the characteristic function of the classical region $R_{\nu(-K,M)}$. Thus, its role in (33) consists essentially in cutting the matrix $\hat{U}^L$ into pieces. The Kirkwood rectangles act on the Kirkwood matrix $\langle p|\hat{U}^L|q\rangle/\langle p|q\rangle$:

$$\mathrm{Tr}(\hat{U}^L\hat{R}_{\nu(-K,M)}) = \sum_{q,p}\langle p|\hat{U}^L|q\rangle\langle q|\hat{R}_{\nu(-K,M)}|p\rangle \approx \frac{1}{N}\sum_{q,p}\frac{\langle p|\hat{U}^L|q\rangle}{\langle p|q\rangle}\chi_{R_{\nu(-K,M)}}(q,p). \tag{35}$$

The coherent rectangles perform a similar action but on the operator symbol $\langle\alpha|\hat{U}^L|\alpha\rangle$:

$$\mathrm{Tr}(\hat{U}^L\hat{R}_{\nu(-K,M)}) \approx \mathrm{Tr}\left(\hat{U}^L\frac{1}{N}\sum_{\alpha\in R_{\nu(-K,M)}}|\alpha\rangle\langle\alpha|\right) = \frac{1}{N}\sum_{\alpha}\langle\alpha|\hat{U}^L|\alpha\rangle\chi_{R_{\nu(-K,M)}}(\alpha). \tag{36}$$

In both cases the semiclassical partial trace is obtained by summing over that piece of the matrix which corresponds to the classical rectangle. Thus each symbolic piece captures the local structure of the propagator in the vicinity of a periodic point labelled by ν and by stationary phase yields the Gutzwiller–Tabor contribution of the corresponding periodic orbit. Forbidden symbols lead to semiclassically small contributions [9].

The symbolic decomposition we have presented has the nice feature of reducing the problem of understanding the asymptotic limit of the traces of the propagator to the analysis of individual 'partial' traces $\mathrm{Tr}\,\hat{U}^L_\nu$, each one characterized by a code given by the symbolic dynamics, and ruled by a periodic point.

We have restricted our discussion to the case of a finite Markov partition. However, the crucial property a partition must display to induce a symbolic dynamics is that of being *generating*, i.e., it must satisfy that, in the limit $K, M \to \infty$, the intersections of (22) are at most points [2]. Moreover, for some semiclassical applications, *any* partition of phase space into small cells may be sufficient [3]. In all cases our method allows us to construct the corresponding quantum partition, and then to obtain an exact symbolic decomposition of the propagators.

4.1. A numerical application

The simplest system in which the quantum partitions can be applied to decompose the propagators is perhaps the baker map [4]. Its Markov partition consists of two rectangles, which, due to the fact that the expanding and contracting directions are parallel to the coordinate axes, are solely defined by conditions on q. As a consequence, the quantum rectangles for the baker map reduce *exactly* to projectors on subspaces [4]. This greatly simplifies the symbolic analysis of the quantum baker map, allowing very detailed studies of its partial traces [4, 10].

However, the baker map is too special for illustrating the properties of the rectangles: many of them are satisfied trivially. Moreover, the partial traces of the baker map display some unpleasant anomalies that difficult the semiclassical analyses [4, 10].

Still simple enough, the Arnold cat map U [11] is more appropriate for a general illustration of the method and can be investigated numerically. The classical cat map is defined by

$$\begin{pmatrix} q' \\ p' \end{pmatrix} = \begin{pmatrix} 2 & 1 \\ 1 & 1 \end{pmatrix}\begin{pmatrix} q \\ p \end{pmatrix} \bmod 1. \tag{37}$$

This is a linear, hyperbolic, and continuous map of the torus. As its invariant manifolds are not aligned with the coordinate axes, the rectangles of the Markov partition [12] (shown in figure 6) are not projectors. This makes the cat map non-trivial for our purposes.

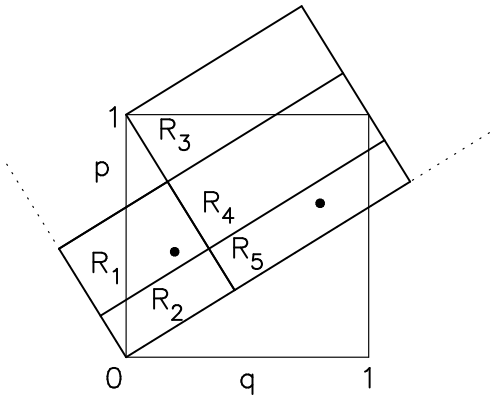

Figure 6. The rectangles $R_1, \ldots, R_5$ constitute a Markov partition of the Arnold cat map. Also shown are parts of the invariant manifolds of the fixed point in the origin (dashed lines), and the period two fixed points with symbolic labels $\nu = 15$ and $\nu = 51$. Here the torus is considered as the plane with points identified if their coordinates differ by integers.

Before proceeding, we must point out that the quantum cat map presents one very particular feature: Gutwiller's semiclassical formula gives the exact traces [13]. For this reason the cat map is not suitable for studying corrections to the trace formula. In principle, any decomposition into partial traces will introduce errors which, however, will cancel out when added up to produce the whole trace. Thus this model may be useful as a test of the mechanisms that lead to such cancellation.

Let us now go to the details of the numerical example. The Markov partition of the cat map consists of the five rectangles of figure 6, which, together with the 'grammar rules' embodied in the transition matrix t,

$$t = \begin{pmatrix} 01001 \\ 01001 \\ 10110 \\ 10110 \\ 10110 \end{pmatrix} \tag{38}$$

define the symbolic dynamics of the cat [12]. Of course, the simplest trace to which our construction can be applied is the first one:

$$\operatorname{Tr} \hat{U} = \sum_{\epsilon_0=1}^{5} \operatorname{Tr}(\hat{U}\hat{R}_{\epsilon_0}). \tag{39}$$

However, the decomposition of this trace does not involve intersections of quantum regions, and thus is not sufficient for illustrating all the workings of the quantum partition. We shall then skip the first trace and concentrate on the decomposition of the second one:

$$\operatorname{Tr} \hat{U}^2 = \sum_{\epsilon_0,\epsilon_1=1}^{5} \operatorname{Tr}(\hat{U}\hat{R}_{\epsilon_0}\hat{U}\hat{R}_{\epsilon_1}). \tag{40}$$

The rectangles $\hat{R}_\epsilon$ are the quantum versions of the regions of figure 6 and can be constructed from either the coherent state representation or Kirkwood's. The construction of the quantum propagator $\hat{U}$ for linear automorphisms of the torus is presented in [14] (notice that Arnold's cat (37) is only quantizable for N even).

Each partial trace can be written asymptotically as a Gutzwiller term plus corrections that go to zero as $N \to \infty$:

$$\operatorname{Tr} \hat{U}_\nu^2 = A_\nu \exp(2\pi \mathrm{i} N S_\nu) + \delta_\nu(N) \tag{41}$$

where A_ν is the amplitude and S_ν the action of the periodic orbit [15]. We remark that in the case of cat maps the corrections δ_ν will cancel out exactly when summing over ν because the

semiclassical trace formula is exact in this special case. In general this will not be true, and the method allows to study the corrections coming from each periodic orbit.

In order to quantify the errors associated to the symbolic partition of the space of paths, we study numerically the semiclassical limit of one element of the partition, namely $\mathrm{Tr}\, U_{51}^2$. This trace is dominated by the periodic trajectory shown in figure 6 and its neighbourhood; its asymptotic limit is the Gutzwiller formula (41) with $A_{51} = 1/\sqrt{5}$ and $S_{51} = \frac{3}{10}$ [16].

We can understand the asymptotic behaviour of the corrections δ_ν by recalling that our decomposition essentially amounts to cutting the matrix of $\hat{U}$ into rectangular blocks. Let us first estimate the corrections in the Kirkwood's case. The Kirkwood matrix of U^L has constant amplitude [14] and phase that oscillates rapidly except in the vicinity of the fixed points of U^L [4]. Computing the partial trace amounts to summing up the matrix elements $\langle p|U^2|q\rangle$ that lie inside the region $R_{51} \equiv R_5 \cap U^{-1}(R_1)$ (shown in figure 5). In the semiclassical limit we can replace the sum by an integration and do the latter using the stationary phase method. In this approximation we must only take into account the contributions of the *critical points* [17]. The most important contribution comes from the the periodic orbit (critical point of the first kind) and its neighbourhood. This gives rise to the Guzwiller term, which is of order zero in $\overline{h}$ ($\mathcal{O}(\overline{h}^0)$). The corrections $\delta_{51}(N)$ are associated to critical points of second and third kind. The critical points of the second kind, i.e., points where the phase is stationary with respect to displacements along the borders of the rectangle, contribute with terms $\mathcal{O}(\overline{h}^{1/2})$. The corners (third-kind critical points) contribute with terms $\mathcal{O}(\overline{h}^{3/2})$. (In the baker map the situation is more complicated because of the coalescence of critical points of a different kind, namely that some fixed points lie on the borders of the rectangles. These anomalous points give rise to terms $\mathcal{O}(\log \overline{h})$ [4,10].) Having exhausted the critical points, we conclude that the border errors in Kirkwood's representation are $\mathcal{O}(\overline{h}^{1/2})$. On the other hand, in the coherent case, one expects the amplitudes $\langle\alpha|\hat{U}^L|\alpha\rangle$ to decay exponentially fast as one moves away from the classical trajectory. The phases do still oscillate fast. However, due to the exponential damping, the border effects in the coherent decomposition should then be $\mathcal{O}[\overline{h}^{1/2}\exp(-C^2/\overline{h})]$, where C is proportional to the distance from the fixed point to the border. Of course, this regime will only be reached once the stationary phase neighbourhood of the fixed point (whose radius is $\mathcal{O}(\overline{h}^{1/2})$) is completely contained in R_{51}.

For the coherent case we calculated numerically the correction δ_{51} as a function of N. Up to $N = 100$ we computed the partial trace exactly, i.e.

$$\frac{1}{N^2}\sum_{\alpha\in R_1,\beta\in R_5}\langle\alpha|\hat{U}|\beta\rangle\langle\beta|\hat{U}|\alpha\rangle. \tag{42}$$

From then on, due to computer time limitations, we resorted to a local semiclassical approximation for the coherent-state propagator. This is equivalent to replacing the torus propagator $\langle\alpha|\hat{U}^2|\beta\rangle$ by a plane propagator which is the quantization of the linear dynamics in the vicinity of the period-two trajectory $\nu = 51$. The errors introduced in this approximation arise from ignoring the contributions of 'sources' located at equivalent (mod 1) positions in the plane [14]. These errors are also $\mathcal{O}[\overline{h}^{1/2}\exp(-C'^2/\overline{h})]$, but with C' much larger than C, and thus can be neglected. Once the partial trace was calculated, we obtained the correction δ_ν by subtracting the Gutzwiller term.

In figure 7 we show the numerical results in a way that permits a direct comparison with our analytical considerations above. In fact, the log–linear plot suggests that the corrections δ_ν in the coherent state decomposition are indeed exponentially small in the semiclassical parameter $1/\overline{h}$. Accordingly, the decomposition which uses rectangles constructed from the Kirkwood representation introduces border errors of order $\overline{h}^{1/2}$; these are the typical diffractive corrections due to sharp boundaries: e.g., like those associated to the passage of a wavefront

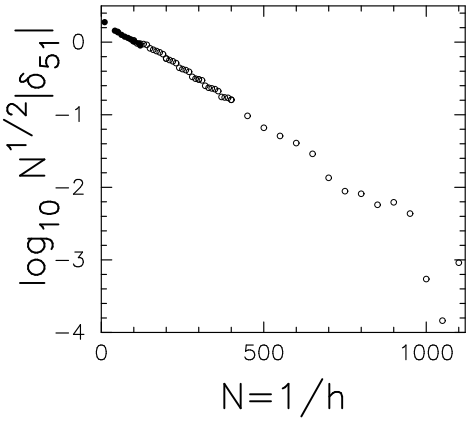

Figure 7. Corrections to the Gutwiller trace formula, $\nu = 51$.

through a hole in a screen (in this case the hole is the classical region and the 'wave' is the mixed representation propagator). We recall that Gutzwiller's trace formula is exact for the cat maps. For typical maps one expects corrections to this formula of order $\overline{h}^k$, with $k \geqslant 1$; e.g., $k = 1$ for the *perturbed* cat maps [18]. Both Markov partitions considered here, either based on coherent-state or Kirkwood rectangles, allow us to study such corrections term by term. In the coherent case, the partitioning of the space of paths does not introduce significant border effects, given that the contributions of neighbouring paths decrease exponentially as one moves away from the central trajectory. On the other hand, the use of a sharp representation like Kirkwood's produces non-negligible boundary contributions to each partial trace. Of course, these boundary terms will cancel out when the partial traces are summed up to give the whole trace. Even so, they have to be carefully identified to isolate the genuine partial corrections to the Gutzwiller trace formula.

5. Concluding remarks

We have begun the application of symbolic dynamics techniques, essential in classical chaotic problems, in quantum mechanics. As a first step we constructed quantum analogues to regions of classical phase space: they are the quantizations of the characteristic functions of the classical regions. We have used Kirkwood's and a coherent state representation. The study of metrical and spectral properties show that they behave asymptotically as projectors over those regions. They also present the diffraction effects typical of ondulatory phenomena.

Even though we only considered a very special phase space (the two-torus), it is clear that our construction can be extended to other quantizable spaces that admit a phase space representation which decomposes the identity.

For a finite-type subshift, the quantization of the rectangles of the classical Markov partition gives rise to a quantum partition which induces a symbolic decomposition of the propagator. This partition allows for writing a trace formula which is both exact and structurally identical to the Gutzwiller trace formula. Thus the problem of understanding the semiclassical limit of the traces of a propagator is reduced to the analysis of partial traces coded by the symbolic dynamics. The objects we have constructed tend asymptotically to their classical counterparts and respond to the same dynamics. In this way, one can verify step by step many manipulations that up to now could only be done at a semiclassical level.

Before concluding we would like to emphasize that the construction presented here is by no means restricted to phase space regions that are Markov partitions. Any region of phase

space selected for 'attention' can be handled in the same way and its quantum properties explored. For example, if a closed problem is turned into a scattering one by the removal of a section of the boundary or the attachment of a soft waveguide, the decomposition leads to the consideration of coupled interior and closure problems projected from the corresponding phase space regions [19]. Another application is to think of the phase space projectors as 'measurements' occurring along the quantum history of the system, and the associated decoherence that results.

Acknowledgments

The authors have benefited from discussions with E Vergini, A Voros and A M Ozorio de Almeida. Critical comments from the referees are also gratefully acknowledged. ROV acknowledges Brazilian agencies FAPERJ and PRONEX for financial support, and the kind hospitality received at the Centro Brasileiro de Pesquisas Físicas and at Laboratorio TANDAR, where part of this work was done. Partial support for this project was obtained from ANPCYT PICT97-01015 and CONICET PIP98-420.

References

[1] Devaney R L 1989 *An Introduction to Chaotic Dynamical Systems* (Redwood City, CA: Addison-Wesley)
[2] Alekseev V M and Yakobson M V 1981 *Phys. Rep.* **75** 287
[3] Bogomolny E B 1992 *Nonlinearity* **5** 805
[4] Saraceno M and Voros A 1994 *Physica* D **79** 206
[5] Saraceno M 1990 *Ann. Phys., NY* **199** 37
[6] Balazs N L and Jennings B K 1984 *Phys. Rep.* **104** 347
[7] Balazs N L and Voros A 1989 *Ann. Phys., NY* **190** 1
[8] Saraceno M and Vallejos R O 1996 *Chaos* **6** 193
[9] Gutzwiller M C 1990 *Chaos in Classical and Quantum Mechanics* (New York: Springer)
[10] Toscano F, Vallejos R O and Saraceno M 1997 *Nonlinearity* **10** 965
[11] Arnold V I and Avez A 1989 *Ergodic Problems of Classical Mechanics* (Reading, MA: Addison-Wesley)
[12] Adler R L and Weiss B 1970 *Mem. Am. Math. Soc.* **98** 1
[13] Keating J P 1991 *Nonlinearity* **4** 277
[14] Hannay J and Berry M V 1980 *Physica* D **1** 267
[15] Tabor M 1988 *Chaos and Integrability in Nonlinear Dynamics* (New York: Wiley)
[16] Keating J P 1991 *Nonlinearity* **4** 309
[17] Mandel L and Wolf E 1995 *Optical Coherence and Quantum Optics* (New York: Cambridge University Press)
Van Kampen N G 1949 *Physica* **14** 575
[18] Boasman P A and Keating J P 1995 *Proc. R. Soc.* A **449** 629
[19] Ozorio de Almeida A M and Vallejos R O 1999 *e-print* chao-dyn/9905010
Ozorio de Almeida A M and Vallejos R O 1999 *e-print* chao-dyn/9905011